CHAPTER 13

Electromagnetic Compatibility

Just as in the preceding chapter, where the magnetic device design must be compatible with system voltages and temperatures, the device must also possess *electromagnetic compatibility*. EMC, the common abbreviated term, is related to EMI, *electromagnetic interference*. Magnetic actuators and sensors must not produce unacceptable EMI, nor have their performance affected adversely by EMI.

13.1 SIGNAL-TO-NOISE RATIO

EMI is electromagnetic interference or noise, where noise is any undesirable signal [1]. There are four general types of EMI.

- **Conducted emissions** are noises produced by the magnetic device that travel to other devices in any system via conductors such as power supply wires.
- **Radiated emissions** are noises produced by the magnetic device that travel to other devices in any system via electromagnetic radiation in air or free space.
- **Conducted susceptance** refers to noises produced in the magnetic device by conduction through wires from other devices.
- **Radiated susceptance** refers to noises produced in the magnetic device by electromagnetic radiation in air or free space.

Whether noise is produced by conduction or radiation, the important factor is whether it dominates the desired signal. For example, if a radio signal, such as a voice and/or music, is large compared with noise, such as static due to lightning, then performance is generally satisfactory. If the noise becomes almost as large as, or larger than, the signal, then performance is usually unsatisfactory. The signal-to-noise ratio, abbreviated as S/N or SNR, is thus a key parameter.

For best S/N, the noise should be reduced and/or the signal increased. If the noise has a different frequency spectrum than the signal, filtering circuits can be employed to reduce the noise. Hence most EMI and EMC specifications by regulatory agencies

Magnetic Actuators and Sensors, Second Edition. John R. Brauer.

(such as the Federal Communications Commission in USA) are in terms of frequency. However, if noise occupies the same frequency band as the signal, then other methods must be used such as digital signal processing and adaptive filters.

Conducted noise can usually be reduced by proper circuit design. For example, conducted noise due to *IR* voltage drops caused by current pulses in an actuator coil can be reduced if the wires from the power supply to the actuator and other devices are large enough to reduce the resistance and if proper grounding is employed [1, 2]. For automotive conducted susceptibility the biggest challenge often is alternator *load dump*, but careful filtering and shielding can prevent it from causing malfunction of proximity sensors [3].

Radiated noise is usually a more difficult problem, whether the magnetic device is emitting it or subjected to it. Magnetic actuators, which often have large ampere-turns, tend to emit EMI. Magnetic sensors, which often are very sensitive to magnetic fields, tend to be very susceptible to EMI.

Inductive magnetic sensors are especially susceptible to radiated EMI. For example, inductive pickup coils of the velocity sensors of Section 11.1 induce voltages proportional to frequency according to Faraday's law. Thus high frequency EMI can induce large noise voltages, larger than the desired signal at low speeds. In automotive EMI engineering [4] involving such velocity sensors on all four wheels, one method of noise suppression is to connect the four sensors so that *common-mode noise* voltages induced in all four wheels essentially cancel out, leaving mostly the desired signal voltage [5].

13.2 SHIELDS AND APERTURES

The best way to reduce radiated emissions and radiated susceptance is to use a *shield*. A shield is a highly conductive enclosure, almost always made of metal. Ideally, it would *completely* enclose and seal off the magnetic actuator or sensor without interfering with its operation.

From Chapter 8, conductive materials possess the skin depth:

$$\delta = \frac{1}{\sqrt{\pi f \mu \sigma}} \tag{13.1}$$

where f is frequency in Hz, μ is permeability, and σ is electrical conductivity. The key parameter in a shield is the ratio of its thickness T to skin depth. The larger the ratio, the lower is the transmissibility of electromagnetic fields from one side of the shield to the other. Thus the larger the ratio of T to skin depth, the better the shield is at preventing EMI.

Shield thickness T equals skin depth at a frequency $f_{\min}$ found from (13.1):

$$f_{\min} = \frac{1}{\pi \mu \sigma T^2} \tag{13.2}$$

For noise frequencies below the minimum frequency $f_{\min}$ the shield is ineffective. Note that for lowest $f_{\min}$, the conductivity, permeability, and thickness should all be as high as possible.

Shield thickness is limited by weight, size, and cost considerations. To reduce the weight, aluminum is a very common shield material. However, the higher permeability of steel causes it to be chosen sometimes to shield low frequencies. In fact, it will be shown that steel shields even reduce DC magnetic field transmission from one side to the other.

For magnetic actuators and sensors, magnetic field EMI is usually the main concern, rather than electric field EMI. However, above a certain frequency range *coupled electromagnetic* radiation, mentioned in Chapter 2, becomes the most significant form of EMI. Thus electric fields are also important, and in fact are usually measured during EMC tests. The frequency at which coupled electromagnetic fields become significant is when the component size, including the shield size, has a dimension of approximately 10% of a wavelength. Wavelength λ is given by:

$$\lambda = c/f \tag{13.3}$$

where c is the speed of light that equals 3.E8 m/s in air or free space.

Unfortunately, almost all shields must contain at least one *aperture*, a term meaning opening or hole. For magnetic sensors, the object or field to be sensed cannot be entirely separated from the sensor, so an aperture is usually required. An example of magnetic sensor with shields is the spin-valve GMR sensor in Figure 10.6, where the shields are above and below, leaving apertures around all the sides. For magnetic actuators, the object to be moved must usually be accessible and thus an aperture is required. For both magnetic actuators and sensors, electrical voltages or currents must be accessed through some sort of terminal.

A typical shield and aperture are shown in Figure 13.1. The shield is a rectangular box with a top piece that is attached above a gasket [6, 7]. To reduce computer modeling time, only one-fourth of the box is needed. The shield has a conductivity

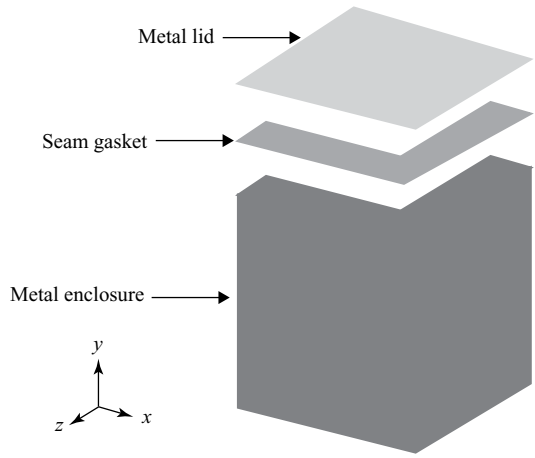

FIGURE 13.1 One-quarter of a rectangular shielding box that is 1 mm thick. The quadrant size is 110 × 110 mm of the 440-mm^2 box. The box height is 115 mm, on top of which is the 5-mm thick gasket and the 1-mm thick lid.

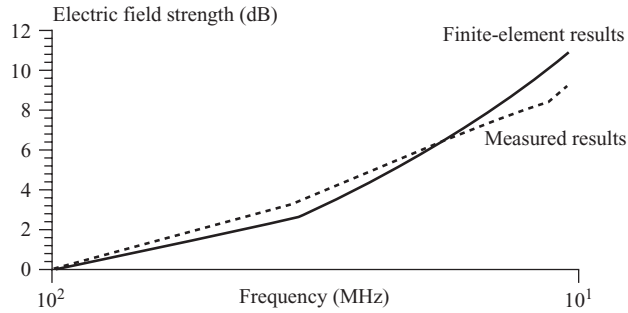

FIGURE 13.2 Computed and measured leakage electric field from shield of Figure 13.1.

of 4.8E7 S/m and the gasket has a complex relative permeability of 100–*j* 100 along with a relative permittivity of 10. Inside the box is a vertically oriented half-loop current source lying in the $x = 0$ plane. The top of the loop is located 50 mm down from the top of the lid. The electric field outside the box is to be computed over the frequency range 100 kHz–100 MHz. At 100 MHz, the wavelength from (13.3) is 3 m. Since the box has maximum dimension of almost 0.5 m, coupled electromagnetic fields can be significant in the range of about 60 MHz and higher. Thus a coupled 3D electromagnetic finite-element formulation, to be presented in the next chapter, was used in all computations for Figure 13.1.

The computed electric field intensity versus frequency is plotted in Figure 13.2, where it is shown to compare fairly closely with measurements available to 1 MHz [6, 7]. Note that the field is plotted in decibels (dB) because of the large amplitude range of electric and magnetic fields (as in Figure 10.1). The computed 3D electric field distribution in three cut planes around the box is displayed in Figure 13.3.

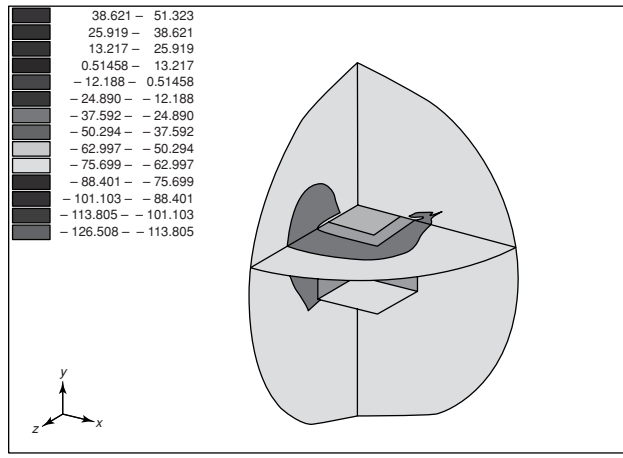

FIGURE 13.3 Computer display of computed electric field distribution in dB emitted by shield of Figure 13.1 at 1 MHz. This display appears in color on the computer screen but is here shown in black and white.

Similar finite-element computations have been carried out for over 100 apertures at frequencies as high as approximately 10 GHz [8].

Some magnetic actuators and sensors inherently possess some shielding. For example, axisymmetric plunger actuators in Chapter 7 almost completely surround their coils by steel, and thus usually emit less EMI than planar actuators with clapper armatures.

Example 13.1 Cylindrical Shield without and with an Aperture A circular copper wire loop carrying 1000 ampere-turns AC is shielded by a cylindrical metal can as shown in Figure E13.1.1. The coil is stranded such that its skin and proximity effects are negligible; its inner radius is 1 mm, outer radius 2 mm, and its height is 1 mm. The coil is centered in the can of inner radius 3 mm, inner height 3 mm, and thickness 0.4 mm. The can has an optional 1-mm airgap below its top. Use finite elements to find the magnetic flux density just inside and outside the top corner of the can for the following cases.

(a) Aluminum can at 60 Hz and 10 kHz with no airgap. The aluminum electrical conductivity is 3.6E7 S/m.
(b) Aluminum can at 10 kHz with 1-mm airgap.
(c) Steel can at 0.1 Hz (essentially DC) and 10 kHz. The steel has relative permeability of 1000 and electrical conductivity 2.E6 S/m.
(d) Steel can at 10 kHz with 1-mm airgap.

Solution Since the overall shield size at the frequencies to be analyzed is much less than 10% of a wavelength, Maxwell's "Eddy Current" solver will be used. Under

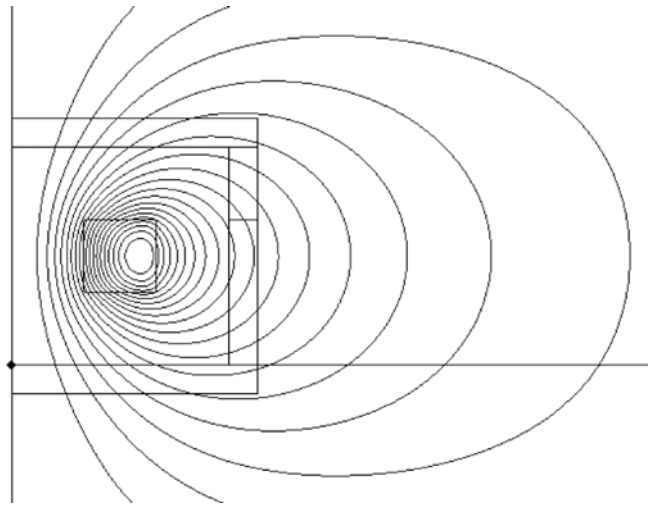

FIGURE E13.1.1 Computer display of cylindrical can with computed flux lines at 60 Hz with complete aluminum shield.

"Sources and Boundary Conditions" use a balloon outer boundary and stranded source. Results are as follows.

(a) At 60 Hz the aluminum is not a good shield, as shown by its flux lines in Figure E13.1.1. Note that they pass through the aluminum as if it were not present, because the skin depth in aluminum at 60 Hz using (13.1) is 10.8 mm, much greater than the shield thickness. Flux densities at the top right inner edge of the can are 0.029 T inside and 0.021 T outside, essentially natural decay with distance. At 10 kHz, some shielding occurs, because the skin depth is now 0.84 mm. The flux densities are 0.031 T inside and 0.015 T outside.

(b) When the aperture is cut in the aluminum, there is more flux density outside. The flux density decays from 0.035 T inside the aperture to 0.020 T outside.

(c) The skin depth in the steel is 0.113 mm at 10 kHz, less than the 0.4-mm thick shield. At 0.1 Hz, B is 1.1 mT just inside the shield and only 0.577 mT outside the shield; the shield itself has flux densities on the order of 0.6 T. At 10 kHz, B is 3.77 mT just inside the shield and only 0.163 mT outside the shield; the shield itself has inner flux densities of 1.6 T. The flux line plot is shown in Figure E13.1.2, and shows how the shield confines most of the magnetic flux.

(d) Cutting the aperture produces 97 mT in the same outside location that previously had only 0.163 mT. As shown in Figure E13.1.3, the aperture allows a lot of flux to pass, although the shield still is helpful.

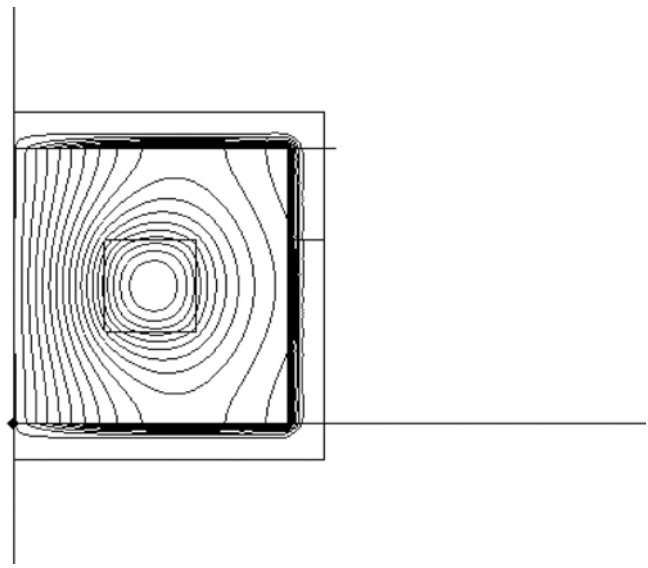

FIGURE E13.1.2 Computer display of cylindrical can with computed flux lines at 10 kHz with complete steel shield.

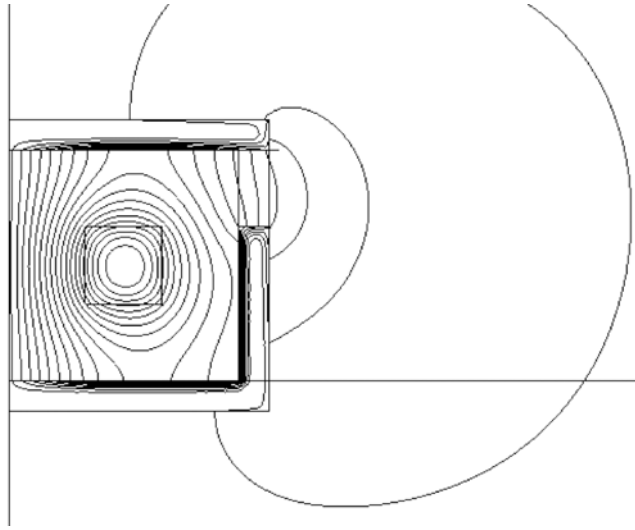

FIGURE E13.1.3 Computer display of cylindrical can with computed flux lines at 10 kHz with steel sheet with an aperture.

13.3 TEST CHAMBERS

Test chambers are commonly used to test radiated EMC behavior of magnetic actuators and sensors. To evaluate emissions, electromagnetic *absorption chambers* are often used. They are quite expensive and large, because they must contain a great deal of absorptive (also called electromagnetic anechoic) material, usually wedge-shaped pieces facing the emitting device. They absorb rather than reflect EMI, and thus simulate the "open air" environment in which many magnetic devices are placed. Smaller, less expensive chambers called transverse electromagnetic (*TEM*) *cells* and *triplate cells* are often used to determine radiated susceptibility.

13.3.1 TEM Transmission Lines

A TEM field has **E** and **H** vectors both lying in the plane transverse (perpendicular or normal to) the direction of energy propagation. **E** and **H** are perpendicular to each other, and the ratio of their magnitudes is called the wave impedance:

$$Z_w = |E_F|/|H_F| = \sqrt{\mu/\varepsilon} \tag{13.4}$$

where the energy is propagating in the forward (F) direction in a lossless material with permeability μ and permittivity ε. Note that the subscript F on E and H indicates the forward-traveling "waves" of E and H. Substituting the material properties of air, its $Z_w = 377\ \Omega$. Assuming no reflections or losses, the only components of **E** and **H** are those in (13.4), and thus the **E** and **H** fields are uniform and known.

TEM cells and triplate cells are basically modified *transmission lines*. A common basic TEM transmission line is a coaxial cable. It is essentially lossless, and has a characteristic impedance commonly denoted as Z_o, given by:

$$Z_o = |V_F|/|I_F| = \sqrt{L/C} \tag{13.5}$$

where V_F is the forward-traveling voltage wave and I_F is the forward-traveling current wave. Also, L is the transmission line inductance per unit length in henrys per meter and C is the transmission line capacitance per unit length in farads per meter. Typical coax (coaxial cable) Z_o values are 50 and 75 Ω. If a coax cable is matched with an impedance (including a Thevenin impedance) on its end equal to its Z_o, then no reflections occur and the only voltages and currents are V_F and I_F. Thus impedance matching produces uniform and known V and I, as well as uniform and known **E** and **H**.

A coax cable has a grounded outer shield and a center conductor. The center conductor usually carries the signal voltage. The current passes down the center conductor and returns via the outer shield. The characteristic impedance can be altered by changing L and C. They are changed by the following.

(a) Changing the material between the shield and the center conductor. For example, different plastics have different permittivities.
(b) Changing the geometry of the center conductor and outer shield. For circular coax, varying these two radii changes Z_o. For other shapes, such as elliptical or rectangular, other values of Z_o can be obtained. Changing the geometry changes both L and C. It is possible, however, to vary the geometry along a transmission line and yet obtain the same L/C ratio, thereby maintaining a constant Z_o. Maintaining constant Z_o prevents reflections, thereby helping to maintain the desired uniform and known V, I, and **E**, **H**.

Besides the above lossless transmission line, lossy (with loss) transmission lines also occur. Their characteristic impedance is given by [9]:

$$Z_o = |V_F|/|I_F| = \sqrt{(R + j\omega L)/(G + j\omega C)} \tag{13.6}$$

where R is the series resistance per unit length in ohms per meter, and G is the parallel conductance per unit length in siemens per meter. Because j is the square root of minus 1, the characteristic impedance in the lossy case can be a complex number. The angular frequency $\omega = 2\pi f$, where f is the frequency in hertz.

In TEM transmission lines, the electric and magnetic fields are at right angles to each other and can be computed separately. If lossless, electrostatic and magnetostatic solutions apply. If lossy, the magnetic field computations should include eddy current losses at the frequency f as described in the preceding chapter.

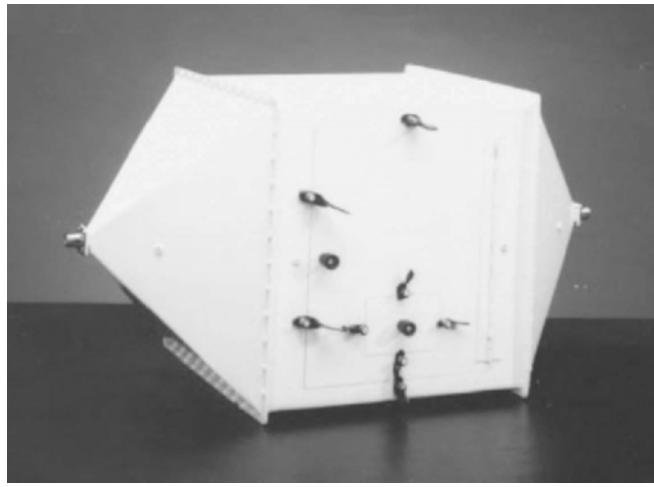

FIGURE 13.4 Typical small TEM cell (33 × 33 × 64 cm).

13.3.2 TEM Cells

A TEM cell is a TEM transmission line that has a big "bulge" in it that serves as the cell or chamber for the device under test. There are many ways to make the "bulge" and thus many varieties and sizes of TEM cells exist. Figure 13.4 shows a typical small TEM cell. Note that the coax connectors on both ends are visible.

Note also in Figure 13.4 that the TEM cell is completely enclosed. However, Figure 13.4 shows that doors are placed in the enclosure walls to allow the device being tested to be inserted. Also couplings through the doors and walls enable measurements of the fields and the device performance.

Interiors of TEM cells can be of various designs. The field is only approximately uniform throughout the entire interior.

13.3.3 Triplate Cells

A triplate cell is a simplification of a TEM cell in which some walls are removed to create three metal "plates." The device to be tested can thus be easily inserted and altered. The triplate in Figure 13.5 has the coax connectors visible on both ends.

Both triplate cells and TEM cells bombard the device under test with both electric and magnetic fields. To find the ratio *E/H* for an arbitrary-shaped triplate or TEM cell, assume that the load impedance on the cell end matches the characteristic impedance, giving $V/I = Z_o$. Then from (13.5):

$$V/I = (L/C)^{1/2} \tag{13.7}$$

$$V^2/I^2 = L/C \tag{13.8}$$

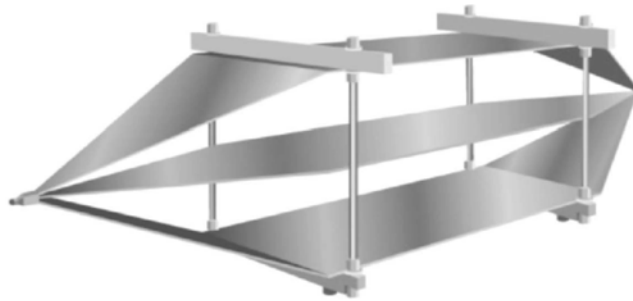

FIGURE 13.5 Typical triplate cell.

Substituting energy expressions (6.17) and (6.23) gives:

$$V^2/I^2 = (2W_{\text{mag}}/I^2)/(2W_{\text{el}}/V^2) \tag{13.9}$$

Thus

$$W_{\text{mag}} = W_{\text{el}} \tag{13.10}$$

This equality has been verified using finite-element computations. Thus a feature of a matched triplate or TEM cell is that its *electric and magnetic fields have equal energies.*

Now the magnetic energy W_{mag} is the volume integral of magnetic energy density, or the average magnetic energy density times the volume:

$$W_{\text{mag}} = (1/2)\mu_o H_{\text{ave}}^2 v \tag{13.11}$$

where H_{ave} is the average H and v is volume. The electric energy is the volume integral of electric energy density, or the average electric energy density times the volume:

$$W_{\text{el}} = (1/2)\varepsilon_o E_{\text{ave}}^2 v \tag{13.12}$$

where E_{ave} is the average E.

Substituting (13.11) and (13.12) into (13.10) gives:

$$(1/2)\mu_o H_{\text{ave}}^2 = (1/2)\varepsilon_o E_{\text{ave}}^2 \tag{13.13}$$

Hence

$$E_{\text{ave}}/H_{\text{ave}} = (\mu_o/\varepsilon_o)^{1/2} = 377 \tag{13.14}$$

Thus in any triplate cell or TEM cell that has a load equal to its characteristic impedance, that is $V/I = Z_o$, the average ratio of E/H is 377. Since the voltage contours (for the **E** field) and the magnetic flux lines are identical as discussed in

the example below, **E** and **H** fields obey this ratio everywhere in matched triplate cells and TEM cells. Most commercial cells produce a specified **E** field, but (13.14) obtains the cell **B** field magnitude as:

$$B = \mu_o E/377 \tag{13.15}$$

Since magnetic sensors and actuators are usually more susceptible to **B** field EMI than to **E** field EMI, (13.15) is often useful.

Example 13.2 Characteristic Impedance of Triplate The cross section of the main center section of a triplate cell is shown in Figure E13.2.1. Its dimensions are 60 × 60 cm. Its three plates are all 5 mm thick. Its center plate is 50.8 cm wide. Find its characteristic impedance using Maxwell software. Also find its voltage contours and magnetic flux lines, assuming it is matched, thereby indicating the variation of the fields over the cell cross section.

Solution To find characteristic impedance using the above formulas, L and C must be found. First, Maxwell's "Electrostatic" solver is used to find C and the electric field. Figure E13.2.1 shows computed voltage contours for $V = 10$ V between the adjacent plates. In most regions $E = V/d = 33.3$ V/m in the vertical direction. However, near the corners of the plates E is much higher, and away from the plates E decays and changes direction ("fringes"). Maxwell also computes the electric energy stored W_E as 2.2564E–9 J/m for $V = 10$ V between the plates. Then from the capacitance energy formula (6.23), solving for capacitance gives:

$$C = 2W_{\text{el}}/V^2 \tag{E13.2.1}$$

the capacitance C is found to be 45.13 pF/m.

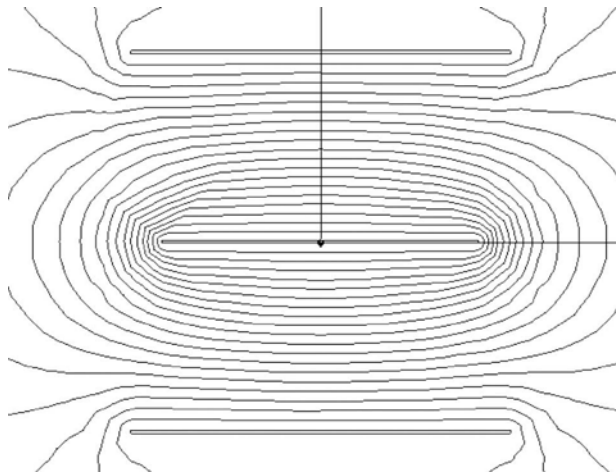

FIGURE E13.2.1 Computer display of triplate cell center cross section and its computed voltage contours or magnetic flux lines.

Next, the same triplate was analyzed for its magnetic fields and inductance using Maxwell's "Eddy Current" solver. To include skin effects expected at audio frequencies (20– 20 kHz) and higher, the plates are assumed to have their currents on their skin, and thus the plate permeability is assumed to be 0.1% that of air. The computed magnetic flux lines appear identical to Figure E13.1.1. For 10 A, the computed magnetic energy is 1.2513E–5 J/m depth. Then from the well-known magnetic energy formula (6.17), solving for inductance gives:

$$L = 2W_{\text{mag}}/I^2 \tag{E13.2.2}$$

the inductance L is found as 250.3 nH/m. Then from (13.5), the characteristic impedance of the triplate is 74.5 Ω. This agrees reasonably well with the 75 Ω specified by the triplate manufacturer.

The magnetic flux lines and voltage contours of Figure E13.1.1 show that a large area of the region between the plates has an approximately uniform field. The field is uniform in most locations away from plate corners. Thus, in using triplate cells, the magnetic device under test must be considerably smaller than the cell and should be placed near the center of the cell. If desired, finite-element models of the device under test can be developed [10] and included in the model of the cell.

PROBLEMS

13.1 Redo Example 13.1 at a frequency of 20 kHz.

13.2 Redo Example 13.1 for steel with a relative permeability of 500 and conductivity 1.5E6 S/m.

13.3 Redo Example 13.2 when the center plate is expanded to the same width as the top and bottom plates.

13.4 Redo Example 13.2 when the top and bottom plates are expanded to 75 cm wide.

13.5 Redo Example 13.2 when the top and bottom plates are 75 cm wide and the center plate is 60 cm wide.

13.6 At a certain distance "down the line" from the center cross section of the triplate cell of Example 13.2 all dimensions are exactly one-half those of the center section. Use Maxwell software to find the characteristic impedance of the smaller section. Also find its voltage contours and magnetic flux lines, assuming it is matched, thereby indicating the variation of the fields over this smaller cross section.

REFERENCES

1. Ott HW. *Noise Reduction Techniques in Electronic Systems*. New York: John Wiley & Sons; 1976.

2. Paul CR. *Introduction to Electromagnetic Compatibility*. New York: John Wiley & Sons; 1992.
3. Repas R. Prox sensors for vehicles. *Machine Design* 2005;37.
4. Markel MS, Brauer JR, Brown BS. Using finite element software to predict automotive EMC. *Proceedings of the EMC/ESD International Conference*, Denver, CO, April 1993.
5. Bauer H (ed.). *Automotive Handbook*, 4th ed. Stuttgart, Germany: Robert Bosch GmbH; 1996, also available from SAE, Warrendale, PA, p 638.
6. Brauer JR, Brown BS. Mixed-dimensional finite elements for models of electromagnetic coupling and shielding. *IEEE Trans Electromagn Compat* 1993;35:235–241.
7. Harada T, Hatakeyama K, Inomata M, Masuda N, Fujihara N. Suppressing electromagnetic field leakage through gaps in metal enclosures using magnetic materials. *Proceedings of the 9th International Zurich Symposium and Technical Exhibition on EMC, Zurich, Switzerland*, March 1991, pp 725–730.
8. Brauer JR. Homogenized finite element model of a beam waveguide resonator antenna with over one hundred coupling holes. *Proceedings of the Applied Computational Electr.omagnetic Society Annual Review of Progress*, Monterey, CA, 1998.
9. Brauer JR. EMC of automotive wiring analyzed by finite elements. Paper presented at *SAE Passenger Car Meeting*, Dearborn, MI, September, 1985; also in *SAE Transactions*.
10. Bracken JE, Bardi I, Mathis A, Polstyanko S, Cendes ZJ. Analysis of system level electromagnetic interference from electronic packages and boards. *Proceedings of the IEEE Meeting on Electrical Performance of Electronic Packaging*, Austin, TX, October, 2005.